Proceedings of the 4th International Conference on Mechatronics and Smart Systems
DOI: 10.54254/2755-2721/2026.34795

Design, Modeling and Finite Element Analysis of an XY Precision Motion Stage Based on Flexure Mechanisms

Lufei Huang

School of Mechanical Engineering and Robotics, Tongji University, Shanghai, China
lyb989121@outlook.com

Abstract. Flexure mechanisms are useful for precision guidance because their motion is generated by elastic deformation rather than sliding contact. This paper presents the design, stiffness modeling and finite element analysis of a flexure-based XY precision motion stage. An ordinary compound parallelogram flexure (CPF) is first modeled using a leaf-flexure stiffness model, and four basic flexure elements are then synthesized by series and parallel relations. Static finite element analysis (FEA) verifies the element stiffness. After correction, the theoretical stiffness of Element 3 is 37912.57 N/m with a relative error of 4.01%, while Element 4 is treated as a series combination of Element 2 units and has the same ideal stiffness as the ordinary CPF. The verified elements are further used to construct a basic XY stage. The ideal parallel-spring estimate gives a stage stiffness of 109.11 N/mm, and FEA gives 103.33 N/mm with very small cross-axis coupling. The results show that the proposed element-based modeling procedure provides a clear route from CPF units to a basic XY compliant stage.

Keywords: flexure mechanism, compound parallelogram flexure, XY precision motion stage, equivalent stiffness, finite element analysis

1. Introduction

Precision positioning stages are widely used in precision manufacturing, optical inspection, micro/nano manipulation and biomedical engineering. Compared with traditional rigid-body guideways, flexure mechanisms achieve motion through elastic deformation, avoiding friction, backlash and wear. Therefore, compliant micro-positioning stages have been widely studied for high-precision motion systems [1, 2].

For XY precision motion, flexure parallelogram mechanisms are commonly adopted because they can provide approximately straight-line translation and good repeatability. Classic studies have proposed large-workspace flexure micropositioning and XY nanopositioning systems [3, 4]. Recent works further improved XY stages through displacement amplification, serial compliant mechanisms, hollow-type structures, parasitic rotation suppression, multi-stage parallelogram flexures and high-bandwidth parallel layouts [5-10]. These studies show that the stiffness and motion accuracy of an XY stage are closely related to the configuration of its flexure modules and the coupling between the two motion directions.

© 2026 The Authors. This is an open access article distributed under the terms of the Creative Commons Attribution License 4.0 (https://creativecommons.org/licenses/by/4.0/).

DOI: 10.54254/2755-2721/2026.34795

In this paper, an XY precision motion stage based on CPF-type flexure mechanisms is designed and analyzed. The stiffness of several basic flexure elements is first derived using beam theory and equivalent spring relations. Then, finite element analysis is used to verify the theoretical stiffness results. Finally, the basic elements are assembled into a symmetric XY stage, and its stiffness, displacement and stress characteristics are evaluated.

2. Design and modeling

2.1. Basic CPF unit

The ordinary compound parallelogram flexure is used as the reference unit. Its equivalent stiffness in the working direction is derived under small-deformation linear elastic assumptions. The schematic in Figure 1 shows the CPF deformation, the loaded leaf flexure and the cross-sectional dimensions.

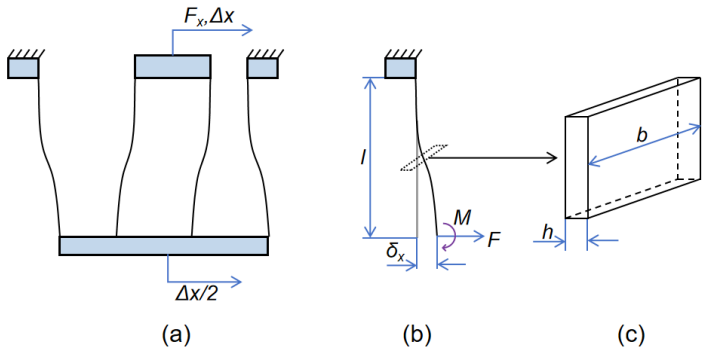


Figure 1. Modeling schematic of the ordinary CPF and leaf flexure: (a) CPF deformation; (b) single leaf flexure under load; (c) cross-sectional dimensions

Let the length, width and thickness of one leaf flexure be l, b and h, respectively, and let E be Young's modulus. The second moment of area I of the rectangular leaf flexure is

$$I = bh^3/12 \tag{1}$$

where h is the thickness in the bending direction. Under a transverse force F and an end moment M, the end rotation constraint and lateral displacement condition are given in (2) and (3), where E is Young's modulus, I is the second moment of area, l is the leaf flexure length, and δ_x is the lateral deflection of one leaf flexure in the working direction.

$$0 = Fl^2/(2EI) - Ml/(EI) \tag{2}$$

$$\delta_x = Fl^3/(3EI) - Ml^2/(2EI) \tag{3}$$

Solving the above equations yields the lateral stiffness of one leaf flexure. For an ordinary CPF, the four leaf flexures have the same geometry. Let Δx be the output displacement of the CPF and F be the total output force. The equivalent stiffness of the ordinary CPF is

$$K^{\mathrm{CPF}} = Ebh^3/\ /l^3 \tag{4}$$

DOI: 10.54254/2755-2721/2026.34795

Thus, the CPF stiffness increases with E, b and h^3, and decreases with l^3. The rigid connecting blocks are treated as ideal rigid bodies, and shear deformation, axial deformation and local compliance at the connections are neglected.

2.2. Stiffness of four basic elements

Four flexure elements are defined based on the ordinary CPF. Only the working-direction stiffness is considered, and the CPF stiffness is used as the reference value.Figure 2 shows the structural schematics of the four basic flexure elements.

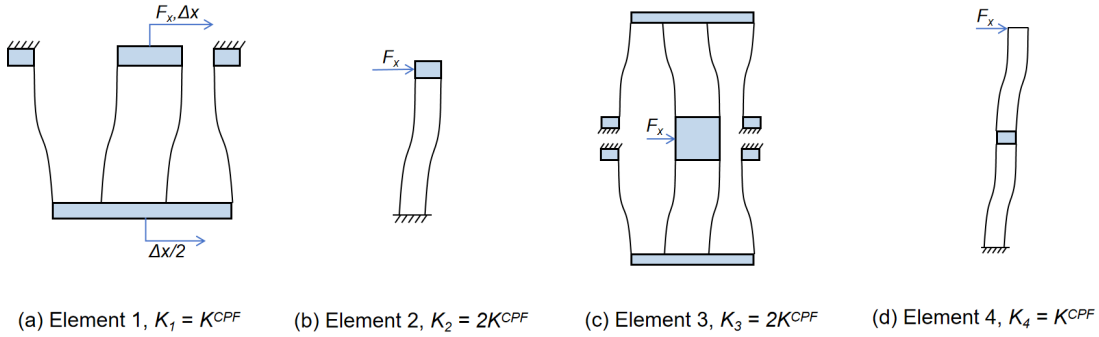


Figure 2. Structural schematics of the four basic flexure elements

Element 1 is the ordinary CPF and serves as the reference element:

$$K_1 = K^{\mathrm{CPF}} \tag{5}$$

Element 2 is obtained from the series-equivalent relation of Element 1. When two identical Element 2 units are connected in series, they are equivalent to one Element 1. Therefore,

$$1/K_1 = 1/K_2 + 1/K_2 \tag{6}$$

$$K_2 = 2K^{\mathrm{CPF}} \tag{7}$$

Element 3 can be regarded as two Element 1 units in parallel. The two branches have the same displacement, and their forces are summed:

$$K_3 = K_1 + K_1 = 2K^{\mathrm{CPF}} \tag{8}$$

Element 4 is modeled as two identical Element 2 units connected in series. Therefore, its equivalent stiffness is

$$K_4 = K_2/2 = K^{\mathrm{CPF}} \tag{9}$$

2.3. Summary of element stiffness

The equivalent stiffness relations of the four elements are summarized in Table 1.

DOI: 10.54254/2755-2721/2026.34795

Table 1. Equivalent stiffness relations of the four basic elements

Element	Structural relation	Basis	Equivalent stiffness
Element 1	Ordinary CPF	Reference unit	K1 = KCPF
Element 2	Series-equivalent to Element 1	Series relation	K2 = 2KCPF
Element 3	Two Element 1 units in parallel	Parallel relation	K3 = 2KCPF
Element 4	Two Element 2 units in series	Series relation	K4 = KCPF

It should be noted that the relation K3 = 2KCPF is an ideal relation based on the standard flexure length l. In the actual Element 3 model used for FEA, the effective flexure length is slightly different and is denoted as l3.This section established the CPF stiffness model and derived the ideal stiffness relations of the four basic elements. The relations are used as the theoretical basis for the finite element verification and the later XY stage design.

3. Finite element verification of the basic elements

ANSYS Mechanical is used to verify the equivalent stiffness model. All four elements are modeled with the same aluminum alloy material, for which Young's modulus is $E = 7.1 \times 10^{10}$ Pa. The leaf flexure dimensions are b = 15 mm, h = 1 mm, and l = 40 mm.

For Element 3, the central rectangular block is longer than the combined side length of the two square blocks. Therefore, the effective flexure length is corrected as l3 = 38.3 mm. Using this corrected length gives K3 = 37912.57 N/m. The theoretical stiffness values used in the simulations are K1 = 16640.63 N/m, K2 = 33281.25 N/m, K3 = 37912.57 N/m, and K4 = 16640.63 N/m.

3.1. Simulation method

Each element is modeled as a three-dimensional solid and analyzed by static structural simulation. The fixed end is fully constrained. A static load from 1N to 10N is applied on the output face along the local Z direction, and the Z-direction displacement of that face is extracted. Here, Z is the local working direction of the element. In the stage model, the elements are rotated so that their local working directions correspond to the global X or Y direction.

All elements use the same meshing strategy. The leaf flexure region is refined, while the rigid connecting blocks use a coarser mesh to reduce the computational cost.Figure 3 illustrates the load constraint, mesh and total deformation setup for Element 1.

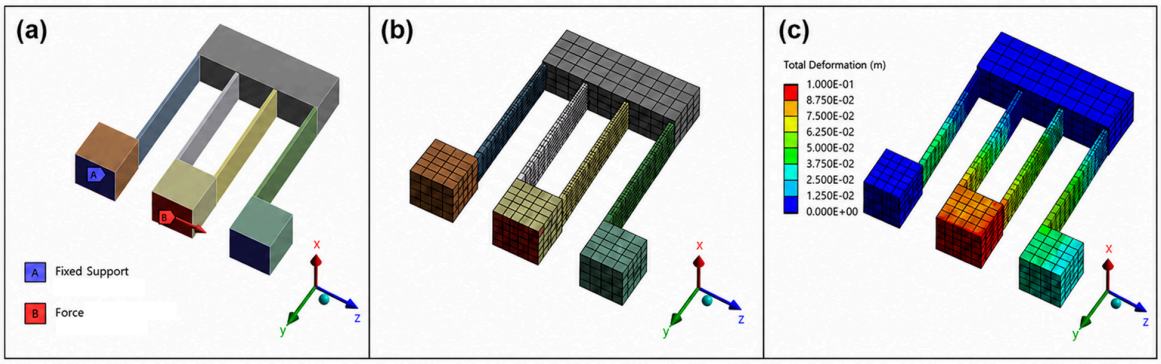


Figure 3. Finite element setup of element 1: (a) load and constraint; (b) mesh; (c) total deformation

DOI: 10.54254/2755-2721/2026.34795

Under the linear elastic small-deformation assumption, load and displacement satisfy

$$F = K\delta \tag{10}$$

In (10), F is the applied load, K is the equivalent stiffness, and δ is the displacement in the local working direction. The theoretical displacement under each load is calculated from the theoretical stiffness. The finite element results are fitted through the origin to obtain the simulated stiffness.

3.2. Results of the four elements

For Element 1, the theoretical stiffness is K1 = 16640.63 N/m, and the fitted FEA stiffness is KFEA = 16875.12 N/m, giving a relative error of 1.41%. For Element 2, K2 = 33281.25 N/m and the fitted stiffness is KFEA = 33908.41 N/m, with an error of 1.88%. For Element 3, the corrected theoretical stiffness is K3 = 37912.57 N/m, while the fitted stiffness reaches KFEA = 39434.23 N/m, giving a relative error of 4.01%. For Element 4, K4 = 16640.63 N/m and the fitted stiffness is KFEA = 16954.21 N/m, with an error of 1.88%.Figure 4 compares the theoretical and FEA load-displacement curves of the four elements.

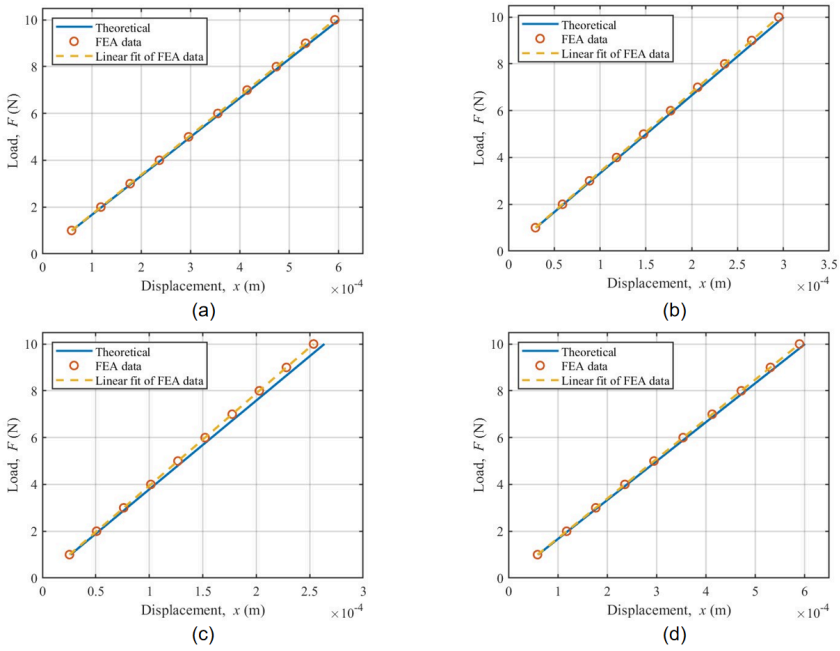


Figure 4. Load-displacement curves of the four elements: (a) Element 1; (b) Element 2; (c) Element 3; (d) Element 4

3.3. Summary of stiffness results

Table 2 lists the theoretical stiffness, simulated stiffness and relative error of the four elements.

Table 2. Comparison between theoretical and simulated stiffness

Element	Theoretical stiffness / N·m⁻¹	FEA stiffness / N·m⁻¹	Relative error / %
Element 1	16640.63	16875.12	1.41
Element 2	33281.25	33908.41	1.88
Element 3	37912.57	39434.23	4.01

DOI: 10.54254/2755-2721/2026.34795

Table 2. (continued)

Element 4	16640.63	16954.21	1.88

All four elements agree well with the corrected theoretical stiffness model. The comparison indicates that the series-parallel stiffness synthesis is suitable for preliminary element design when the effective geometry of the flexures is properly considered.

The four elements show approximately linear load-displacement behavior in the 1 N to 10 N range. The theoretical and simulated stiffness values are close, which supports the use of Elements 3 and 4 in the subsequent XY stage design.

4. Design and finite element analysis of the basic XY stage

After verifying the basic elements, a basic XY precision motion stage is constructed. The stage is first estimated by an ideal parallel-spring model and then evaluated by static finite element simulation. The material is aluminum alloy with $E = 7.1 \times 10^{10}$ Pa and Poisson's ratio $\nu = 0.33$.

4.1. Stage structure

The basic XY stage adopts an orthogonal symmetric layout, as shown in Fig. 5. It consists of a central output platform, four compliant branches and outer fixed supports. The central platform provides the output displacement, while the surrounding branches guide the motion in two perpendicular directions.

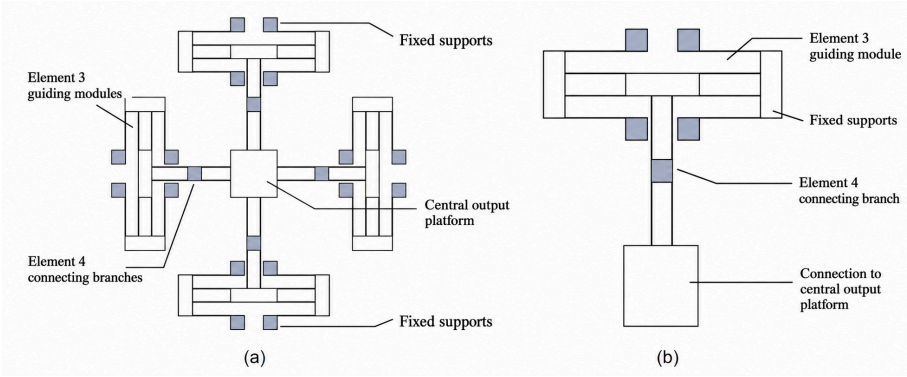


Figure 5. Basic XYprecision motion stage:(a)overall structure;(b)single-branch structure

A single branch consists of an Element 3 guiding module and an Element 4 connecting branch, as shown in Fig. 5(b). Element 3 provides the guiding constraint, while Element 4 connects the guiding module to the central output platform. The repeated branch layout improves structural symmetry and reduces parasitic motion.

The stage transmits motion through elastic deformation of the leaf flexures. Therefore, it avoids sliding friction and backlash in rigid guideways. Under ideal symmetric conditions, the X- and Y-direction responses are expected to be similar.

4.2. Theoretical stiffness estimate of the XY stage

For a first-order estimate, the X- and Y-direction stiffness is simplified as a parallel-spring system. Owing to the symmetric layout, the two directions have the same ideal stiffness. In each direction,

DOI: 10.54254/2755-2721/2026.34795

two Element 3 modules and two Element 4 branches are assumed to work in parallel.

$$K_{x,\mathrm{th}} = K_{y,\mathrm{th}} = 2K_3 + 2K_4 \tag{11}$$

Using the corrected stiffness of Element 3 and the updated stiffness of Element 4, the stage stiffness estimate becomes

$$K_{x,\mathrm{th}} = K_{y,\mathrm{th}} = 2(37912.57) + 2(16640.63) = 1.0911 \times 10^5 \mathrm{N/m} = 109.11 \mathrm{N/mm} \tag{12}$$

This ideal estimate is equal to 109.11 N/mm. It is a first-order estimate because it treats the branches as ideal parallel springs and neglects the flexibility of connecting blocks and the non-ideal deformation path of the complete stage.

The deformation shapes in the finite element plots are amplified for display. The actual motion should be evaluated from the numerical displacement values and load-displacement curve.

4.3. Finite element model and boundary conditions

The static structural setup is shown in Fig. 6. The outer support blocks are fixed to simulate the mounting condition, and two independent loading cases are considered. In Case 1, the load is applied to the central platform in the X direction. In Case 2, the load is applied in the Y direction. The load increases from 1 N to 10 N in both cases.

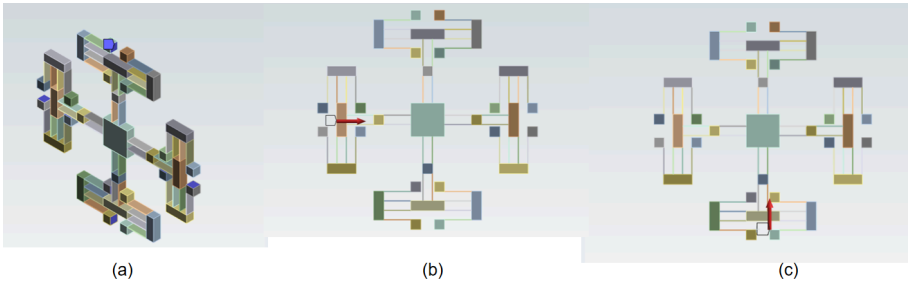


Figure 6. Finite element setup of the XY stage: (a) fixed supports; (b) X-direction loading; (c) Y-direction loading

For each case, the displacement in the main motion direction and the displacement in the perpendicular direction are extracted. Under X-direction loading, the X displacement is the main displacement δm and the Y displacement is the parasitic displacement δp. Under Y-direction loading, the Y displacement is δm and the X displacement is δp.

4.4. Displacement response

The displacement results in Fig. 7 show that the main displacement of the central platform is 9.6774 × 10^{-5} m under both X-direction and Y-direction loading. The close results indicate similar compliant motion capability in the two directions.

DOI: 10.54254/2755-2721/2026.34795

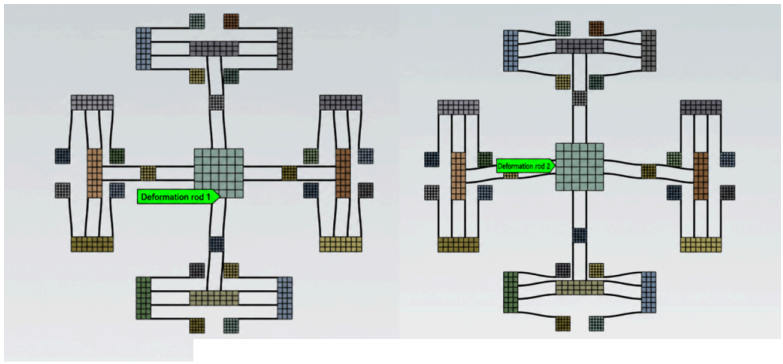


Figure 7. Displacement results of the XY stage: (a) X-direction displacement under X-direction loading; (b) Y-direction displacement under Y-direction loading (deformation amplified)

4.5. Stiffness and coupling analysis

The main-direction load-displacement response is shown in Fig. 8. The horizontal axis denotes the main displacement δm in the loading direction. The theoretical line is calculated from the ideal parallel-spring estimate, while the FEA data points and their fitted line are obtained from the static simulation results.The following analysis first gives the theoretical stiffness, then calculates the FEA stiffness from the load-displacement response, and finally compares the two results.

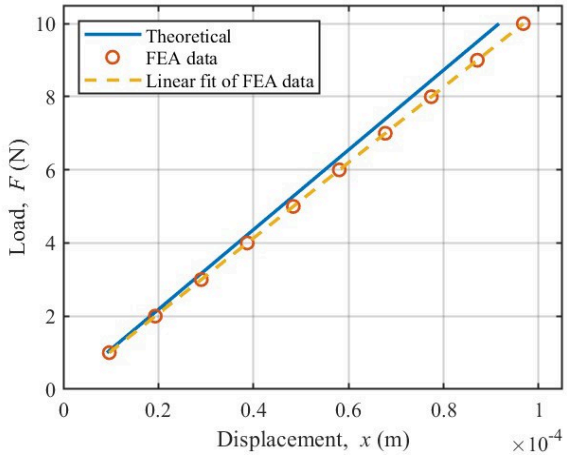


Figure 8. Theoretical and FEA load-displacement comparison of the XY stage

The theoretical stiffness obtained from the ideal parallel-spring model is given by (12). This value is used as a first-order theoretical estimate. The FEA equivalent stiffness in the main motion direction is then calculated by

$$K_{\mathrm{FEA}} = F/\delta_m \tag{13}$$

where F is the applied load and δm is the main displacement of the central platform. For the 10 N case,

$$K_{x,\mathrm{FEA}} = K_{y,\mathrm{FEA}} = 10/\left(9.6774 \times 10^{-5}\right) = 1.0333 \times 10^{5}\mathrm{N/m} = 103.33\mathrm{N/mm} \tag{14}$$

DOI: 10.54254/2755-2721/2026.34795

The theoretical stiffness is K_{th} = 109.11 N/mm, while the FEA stiffness is K_{FEA}= 103.33 N/mm. The relative stiffness error is calculated as

$$e_K = |K_{\mathrm{FEA}} - K_{\mathrm{th}}| / K_{\mathrm{th}} \times 100\% = 5.29\% \tag{15}$$

This difference indicates that the simplified parallel-spring model provides a reasonable first-order prediction, although the actual stage stiffness is reduced by the compliance of connecting blocks and the non-ideal deformation path. The theoretical and FEA results are summarized in Table 3.

The coupling ratio is defined as

$$\eta = |\delta_p| / |\delta_m| \times 100\% \tag{16}$$

where $\delta_p$is the parasitic displacement and δ_m is the main displacement. The absolute value is used because the parasitic displacement may have different signs depending on the direction. At 10 N, δ_m = 9.6774 × 10^{-5} m and δ_p = 3.5097 × 10^{-9} m, giving

$$\eta = \left(3.5097 \times 10^{-9}\right) / \left(9.6774 \times 10^{-5}\right) \times 100\% = 0.0036\% \tag{17}$$

Thus, under ideal geometry, ideal boundary conditions and linear elastic assumptions, the parasitic displacement is much smaller than the main displacement. In practice, machining and assembly errors may increase the coupling. The maximum equivalent stress from the representative 10 N loading case is also included in Table 3.

Table 3. Theoretical and FEA results of the basic XY stage

Loadingcase	K_{th}(N/mm)	K_{FEA} (N/mm)	Error(%)	δ_m (m)	δ_p (m)	η (%)	σ_{max}(MPa)
X loading	109.11	103.33	5.29	9.6774×10^{-5}	3.5097×10^{-9}	0.0036	7.2133
Y loading	109.11	103.33	5.29	9.6774×10^{-5}	3.5097×10^{-9}	0.0036	7.2133

4.6. Equivalent stress analysis

A representative von Mises stress distribution under a 10 N load is shown in Fig. 9. Because the stage is symmetric, the stress distribution trends under X- and Y-direction loading are similar.

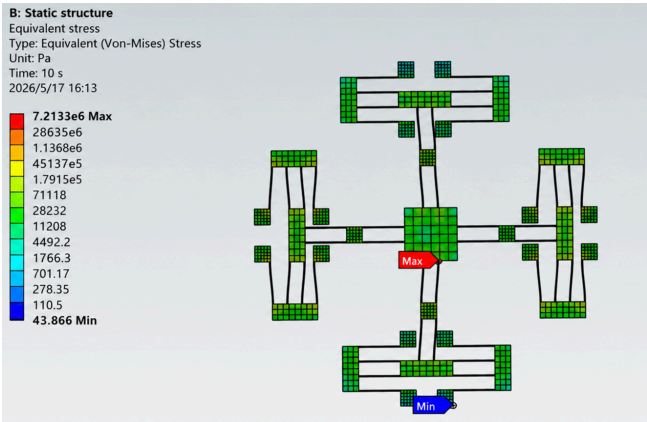


Figure 9. Representative equivalent stress distribution under 10 N loading

DOI: 10.54254/2755-2721/2026.34795

The maximum equivalent stress is 7.2133 MPa and is mainly located in the compliant branches and connecting regions. The central platform and outer fixed blocks have lower stress and mainly serve as motion transmission and support regions. The stress level is far below the typical yield strength of common aluminum alloys, so the stage is expected to remain in the elastic range under the considered static loads.

4.7. Summary

This section designed and analyzed a basic XY precision motion stage. The finite element results show similar X- and Y-direction responses, low parasitic displacement and a safe stress level under the considered static load range. The theoretical parallel-spring estimate provides an ideal reference, while the FEA result reflects the compliance of the complete stage.

5. Conclusions and future work

5.1. Conclusions

This paper developed a flexure-based XY precision motion stage through element-level modeling, finite element verification and stage-level analysis. The ordinary CPF was used as the reference unit, and four basic flexure elements were derived through ideal series and parallel stiffness relations.

The finite element results show that the four elements agree well with the theoretical stiffness model in the 1 N to 10 N range after the effective length correction for Element 3. This result shows that simplified stiffness models are useful for preliminary design, but local geometric details must be considered when the structure differs from the ideal model.

A basic XY compliant stage was constructed using Element 3 guiding modules and Element 4 connecting branches. The stage exhibits similar X- and Y-direction responses, small parasitic displacement and low stress under ideal geometric and boundary conditions. The FEA stiffness is lower than the corrected ideal parallel-spring estimate, which is reasonable because the complete stage includes non-ideal load paths and local compliance.

5.2. Future work

The present work remains a structural design and simulation study. Future work should optimize the branch dimensions, include actuator and sensor integration, and evaluate the effects of machining error, assembly error and dynamic behavior. Prototype fabrication and experimental testing are also required to validate the model and improve the design for practical precision positioning applications.

References

[1] Bingxiao Ding; Xuan Li; Chenglin Li; Yangmin Li; Shih-Chi Chen. A survey on the mechanical design for piezo-actuated compliant micro-positioning stages [J]. Review of Scientific Instruments, 2023, Vol.94(10): 101502.

[2] Mingxiang Ling; Larry L. Howell; Junyi Cao; Guimin Chen. Kinetostatic and dynamic modeling of flexure-based compliant mechanisms: A survey [J]. Applied Mechanics Reviews, 2020, Vol.72(3): 030802.

[3] Qingsong Xu. New flexure parallel-kinematic micropositioning system with large workspace [J]. IEEE Transactions on Robotics, 2012, Vol.28(2): 478-491.

[4] Shorya Awtar; Gaurav Parmar. Design of a large range XY nanopositioning system [J]. Journal of Mechanisms and Robotics, 2013, Vol.5(2): 021008.

DOI: 10.54254/2755-2721/2026.34795

[5] Haitao Wu; Leijie Lai; Liqiang Zhang; Limin Zhu. A novel compliant XY micro-positioning stage using bridge-type displacement amplifier embedded with Scott-Russell mechanism [J]. Precision Engineering, 2022, Vol.73: 284-295.
[6] Philipp Gräser; Sebastian Linß; Felix Harfensteller; Mario Torres; Lena Zentner; René Theska. High-precision and large-stroke XY micropositioning stage based on serially arranged compliant mechanisms with flexure hinges [J]. Precision Engineering, 2021, Vol.72: 469-479.
[7] Lusheng Yuan; Liang Wang; Rui Qi; Zhenhua Zhao; Jiamei Jin; Chunsheng Zhao. A novel hollow-type XY piezoelectric positioning platform [J]. International Journal of Mechanical Sciences, 2023, Vol.255: 108496.
[8] Yijie Liu; Zhen Zhang. A large range compliant XY nano-manipulator with active parasitic rotation rejection [J]. Precision Engineering, 2021, Vol.72: 640-652.
[9] Zekui Lyu; Qingsong Xu. Design and testing of a large-workspace XY compliant manipulator based on triple-stage parallelogram flexure [J]. Mechanism and Machine Theory, 2023, Vol.184: 105287.
[10] Tingwei Wang; Yingzi Li; Yingxu Zhang; Rui Lin; Jianqiang Qian; Zhipeng Dou. Design of a flexure-based parallel XY micropositioning stage with millimeter workspace and high bandwidth [J]. Sensors and Actuators A: Physical, 2021, Vol.331: 112899.